Structural Eng./Earthquake Eng., JSCE, Vol. 15, No. 1, 19s—27s, 1998 January
(J. Struct. Mech. Earthquake Eng., JSCE, No. 584/ I —42)

2D NONLINEAR SEISMIC GROUND ANALYSIS BY FEM-BEM: THE CASE OF KOBE IN THE HYOGO-KEN NANBU EARTHQUAKE

Hirokazu TAKEMIYA[1] and Maher ADAM[2]

[1]Member of JSCE, Dr. of Eng., Professor, Dept. of Environmental and Civil Eng. , Okayama University, (Tsushima-Naka, 3-1-1, Okayama, 700, Japan)

[2]Member of JSCE, M. Eng., Ph.D. Formerly, graduate student
Lecturer, Dept. of Civil Engineering, Zagazig University, Cairo, Egypt

The Hyogo-ken Nanbu Earthquake (Jan. 17, 1995) caused devastating damages in and around Kobe city. Noteworthy is the fact that the heaviest damages of JMA intensity 7 were centered in the so-called "disaster belt zone" along the coast. The authors, focusing on the geological features in a north-south section of Kobe, have performed the computer simulation for the 2-dimensional in-plane seismic (P and SV) wave propagation based on the FEM-BEM hybrid modeling. The nonlinear soil behavior was emphasized to better interpret the soft alluvium amplification that depends on the given distribution of soil properties in Kobe.

Key Words : *Hyogo-ken Nanbu Earthquake, disaster belt zone, alluvium amplification, nonlinear behavior, time domain FEM-BEM analysis.*

1. INTRODUCTION

In the Hyogo-ken Nanbu Earthquake (1995) a severely damaged belt zone called "Seismic disaster belt of JMA intensity 7" emerged. Ishikawa et.al[1)] gave a detailed site investigation report on this by focusing on the surface geology of Kobe. Many investigators have looked for some clues for the cause in the Kobe's unique geographical and geological features. A survey of these publication has been made in Ref. 2.

In the previous paper,[3),4)] in order to get a firsthand insight into the soil amplification of the seismic waves by the alluvium deposits in Kobe, the authors carried out a linear out-of-plane (SH wave) and in-plane (P and SV waves) response computation for a simple wedge-shaped model. They pointed out a complex wave field in the alluvium as the results of interference between the horizontally and vertically propagating waves that lead a big amplification of the surface response across the seismic disaster belt. Hence, they termed this phenomenon as a "bump effect". However, noticed there is also an unrealistic highly amplified acceleration at the coastal area with less structural damage except for the harbor facilities by liquefaction. In order to overcome this problem, a more realistic distribution of soil properties by

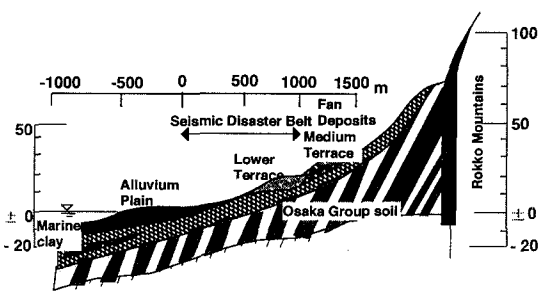

Fig.1 Representative north-south cross section of Kobe[1)]

location is taken into account based on the bore hole test data provided by the Kobe City Office[5)]. **Fig.1** (cited from Ref.1) depicts a representative vertical section of Kobe from the Rokko mountains toward the Inland sea.. Concerning soil deposits profile at the upper 20 m depth, the Holocene clay predominates the coastal area due to the past sea bed sedimentation, whereas the sand and gravely sand soils are accumulated by the river from the damaged area toward the Rokko mountains foot. The soft soils are supposed to have behaved nonlinear hysteric during the strong ground motions in the Hyogo-ken Nanbu Earthquake. Therefore, in what follows such analysis is conducted by extending the previous liner BEM-FEM solution

method[6] amenable to a modified Hardin-Drnevich stress-strain model in the FEM domain. This hybrid method utilizes advantages of the respective discretization methods; namely, the BEM fulfills the infinitely extending boundary condition while the FEM accommodates a given stiffness change by the response level. Then, a system of incremental governing equations are solved for an assumed seismic wave, as a vertical incidence SV incidence, by the Newton-Raphson[7] method with use of the initial stiffness at small strain state. Thus obtained nonlinear results are adequately interpreted in terms of the surface soil amplification of seismic motions in connection to the aforementioned heavy seismic damage belt zone. Comments are also given to a convenient linear analysis with a scaled viscous damping ratio to the nonlinear hysteric response.

2. MODELING OF SOIL NONLINEARITY

Soils exhibit a pronounced nonlinear shear behavior under strong loading which leads decrease of the shear modulus with increase of the shear strain. Under a symmetrical cyclic loading, hysteresis loops are formed by the nature of softening and therefore the material damping, being largely independent of frequency, is produced. If the initial loading curve is described by a function form, the hysteresis loops can easily be constructed on the rule of the Masing's hypothesis[8] to model the behavior under repeated symmetric loading. The shear stress-strain relationship for the Davidenkov-class models is expressed in a generalized form as

$$\tau = \tau_c + G_{max}(\gamma - \gamma_c)\left[1 - H\left(\frac{1}{n}|\gamma - \gamma_c|\right)\right] \qquad (1)$$

in which γ_c and τ_c are the values of shear strain and stress, respectively, at the last reversal under cyclic loading; G_{max} is the initial tangent shear modulus; and **H** is a function that describes the stress- strain relationship. The factor n = 1 is applied for initial loading and n = 2 is for unloading and reloading process.

A simple but meaningful model to represent the soil behavior may be constructed by a hyperbolic function as proposed by Hardin and Drnevich[9]. The stress-strain relationship **H** is then defined by

$$H(\gamma) = \frac{\frac{\gamma}{\gamma_r}}{1 + \frac{\gamma}{\gamma_r}} \qquad (2)$$

where γ_r is a reference strain defined in a quotient of the maximum shear stress τ_{max} of soil in its initial state to the initial tangent modulus G_{max}.

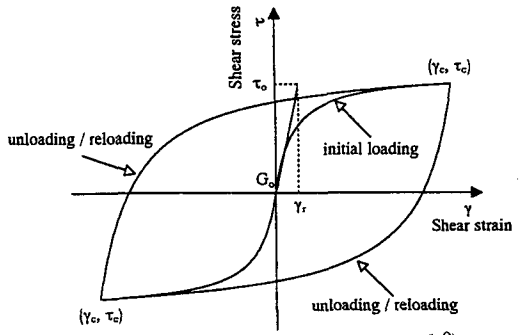

Fig.2 Stress-strain loops for Hardin - Drnevich[9] model

$$\gamma_r = \frac{\tau_{max}}{G_{max}} \qquad (3)$$

In this case the shear stress in Eq.(1) is given by

$$\tau = \tau_c + G_{max}(\gamma - \gamma_c)\left[\frac{1}{1 + \frac{|\gamma - \gamma_c|}{n\gamma_r}}\right] \qquad (4)$$

The skeleton curves and the original Masing's rule lead to hysteresis loops for cyclic loading. Under irregular earthquake loading, on the other hand, some additional criteria are needed to describe the complex behavior. Takemiya and Ishiyama[10] detailed the procedure to implement those rule in the 2-dimensional FEM computer program.

3. NONLINEAR SOLUTION METHOD

The 2-dimensional modeling is made for the surface soils and surrounding far field. The FEM for the former domain takes quadrilateral plane strain elements. The BEM for the latter domain takes linear geometry elements whose displacement and traction are presumed constants over individual element and vary stepwise with time increments. The associated governing equation has a time marching recurrence expression. The FEM equilibrium is also expressed in the dame time marching discrete form[11] but with the finer time step since the explicit presence of inertial force in the governing equation in contrast to the BEM including it implicitly in the Green function priori. Therefore, the BEM time step Δt is divided into N numbers of an equi-time step Δt_f for FEM The coupling of FEM and BEM is performed at Δt (or every N steps) while the governing equation is solved at each time step Δt_f.[12] In reference to the previous linear response analysis,[3),4),6)] the coupled equations of FEM and BEM is formulated where the interface nodes and other remaining nodes are identified by the subscripts I and O, respectively, as

$$\begin{bmatrix} \mathbf{KF_{OO}} & \mathbf{KF_{OI}} \\ \mathbf{KF_{IO}} & \mathbf{KF_{II}}+\Delta t_f^2\alpha\mathbf{K_{BB}} \end{bmatrix} \begin{Bmatrix} \mathbf{u_O} \\ \mathbf{u_I} \end{Bmatrix}^{K+\frac{i}{N}} = \Delta t_f^2 x$$

$$\left[\begin{Bmatrix} 0 \\ \mathbf{RB} \end{Bmatrix}^{K+\frac{i}{N}} - \begin{Bmatrix} 0 \\ \mathbf{RB1} \end{Bmatrix}^{K+\frac{i-1}{N}} \right] + \begin{Bmatrix} \mathbf{RF_O} \\ \mathbf{RF_I} \end{Bmatrix}^{K+\frac{i-1}{N}} + \begin{Bmatrix} \mathbf{RF_O} \\ \mathbf{RF_I} \end{Bmatrix}^{K+\frac{i-2}{N}} \quad (5)$$

with superscript K denoting the BEM step and i the FEM step. The concerned matrices without partitioning are

$$[\mathbf{KF}] = [\ \mathbf{M_F} + \gamma\ \Delta t_f\, \mathbf{C_F} + \beta\, \Delta t_f^2\ \mathbf{K_F}\ ]$$

$$\{\mathbf{RB}\}^{K+\frac{i}{N}} = \alpha \mathbf{F_{BB}}^{K+\frac{i}{N}} + (1-\alpha)\mathbf{F_{BB}}^{K+\frac{i-1}{N}}$$

$$\{\mathbf{RB1}\}^{K+\frac{i}{N}} = (1-\alpha)\mathbf{K_{BB}}\mathbf{u_I}^{K+\frac{i-1}{N}}$$

$$\{\mathbf{RF}\}^{K+\frac{i-1}{N}} = \left[2\mathbf{M_F} - (1-2\gamma)\,\Delta t_f\, \mathbf{C_F} + \left(2\,\beta - \gamma + \frac{1}{2}\right)\Delta t_f^2 \mathbf{K_F}\right] \mathbf{U}^{K+\frac{i-1}{N}}$$

$$\{\mathbf{RF}\}^{K+\frac{i-2}{N}} = \left[-\mathbf{M_F} + (1-\gamma)\,\Delta t_f \mathbf{C_F} + \left(-\beta + \gamma - \frac{1}{2}\right)\Delta t_f^2 \mathbf{K_F}\right] \mathbf{U}^{K+\frac{i-2}{N}}$$

where $\mathbf{M_F}, \mathbf{C_F}$ and $\mathbf{K_F}$ represent respectively the mass, damping and stiffness matrices for the FEM domain, and $\mathbf{K_{BB}}$ the stiffness for the BEM. The coefficients involved for the numerical integration are set to $\alpha=1/2$, $\beta= 1/4$, $\gamma=$ for the use of a linear symmetric weighting function at origin[6]. Suppose the incremental solution is known up to the time step $K+(i-1)/N$, then we can solve Eq.(5) for the next time step $K+i/N$ based on these.

For the nonlinear analysis, the dynamic equilibrium conditions are established to satisfy at each specified incremental times. Takemiya and Ishiyama[10] applied an iterative solution method for the FEM soil dynamic analysis. Herein, the same method is taken with appropriate modification to Eq.(5).

The equilibrium at time t+ Δt ($K+\frac{i}{N}$), given the response at t($K+\frac{i-1}{N}$), is stated as

$$\mathbf{R}^{K+\frac{i}{N}} - \left(\mathbf{F}^{K+\frac{i-1}{N}} + \Delta\mathbf{F}^{K+\frac{i}{N}}\right) = 0 \quad (6)$$

where $\mathbf{R}^{K+\frac{i}{N}}$ denotes the externally applied nodal forces, at t+Δt and $\Delta\mathbf{F}^{K+\frac{i}{N}}$ is the incremental nodal forces corresponding to the generated element stress at this time. The Eq.(6) is solved by taking a step-by-step incremental equilibrium procedure. An assumption for the displacement variation of

$$\mathbf{u}^{K+\frac{i}{N}} = \mathbf{u}^{K+\frac{i-1}{N}} + \Delta\mathbf{u}_{(j)}^{K+\frac{i}{N}} \quad (7)$$

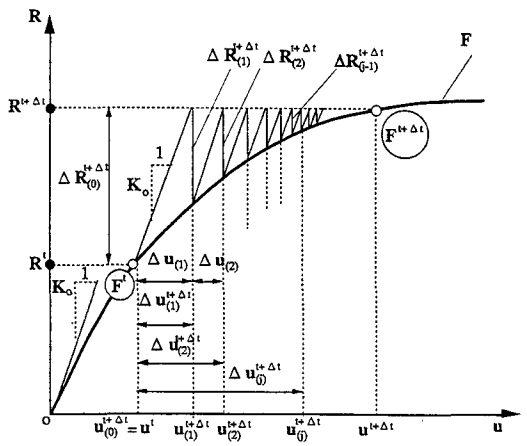

Fig. 3 Modified Newton-Raphson method with use of the initial stiffness

with $\Delta\mathbf{F}^{K+\frac{i}{N}}$, being the incremental nodal point displacement, leads the equilibrium at time t+Δt as

$$\mathbf{K}^{K+\frac{i-1}{N}}\Delta\mathbf{u}^{K+\frac{i}{N}} = \mathbf{R}^{K+\frac{i}{N}} - \mathbf{F}^{K+\frac{i-1}{N}} \quad (8)$$

The Eq.(8) can be solved by iteration method with use of the initial stiffness, which can be formulated as

$$\mathbf{K_0} \sum_{m=1}^{j} \Delta\mathbf{u}_{(m)}^{K+\frac{i}{N}} = \Delta\mathbf{R}_{(0)}^{K+\frac{i}{N}} + \sum_{m=1}^{j-1} \Delta\mathbf{R}_{(m)}^{K+\frac{i}{N}} \quad (9)$$

or

$$\mathbf{K_0}\ \Delta\mathbf{U}_{(j)}^{K+\frac{i}{N}} = \Delta\mathbf{R}_{(0)}^{K+\frac{i}{N}} + \Delta\mathbf{R}_{0(j)}^{K+\frac{i}{N}} \quad (10)$$

in which $\Delta\mathbf{R}_{0(j)}^{K+\frac{i}{N}}$ accounts for the difference between the actual nonlinear stresses and the assumed linear stresses.

$$\Delta\mathbf{R}_{o(j)}^{K+\frac{i}{N}} = -\sum_{e=1}^{elements} \int_{v_e} [\mathbf{B_e}]^T \left\{ \Delta\sigma_{e,u} \right\}_j^{K+\frac{i}{N}} dv_e \quad (11)$$

The out-of-balance stresses $\left\{ \Delta\sigma_{e,u} \right\}_j^{K+\frac{i}{N}}$ is obtained by following the above iterative scheme. The details are explained in Appendix.

The specific expression of Eq.(10), when Eq(5) is used for the governing equation, can be driven as

$$[\mathbf{K_o}]\left\{\Delta\mathbf{u}_{(j)}^{K+\frac{i}{N}}\right\} = \Delta t_f^2 \left[\{\mathbf{RB}\}^{K+\frac{i}{N}} - \{\mathbf{RB1}\}^{K+\frac{i-1}{N}}\right]$$

$$+ \{\mathbf{RF}\}^{K+\frac{i-1}{N}} + \{\mathbf{RF}\}^{K+\frac{i-2}{N}} + \{\Delta\mathbf{Ro}\}_{(j-1)}^{K+\frac{i}{N}} \quad (12)$$

with

$$\{\mathbf{RF}\}^{K+\frac{i-1}{N}} = [\ \mathbf{M}_F - (1-\gamma)\,\Delta t_f\,\mathbf{C}_F\ ]\{\mathbf{u}\}_I^{K+\frac{i-1}{N}} + \left(\beta - \gamma - \frac{1}{2}\right)\Delta t_f^2 \{\mathbf{RS}\}^{K+\frac{i-1}{N}} \quad (13)$$

$$\{\mathbf{RF}\}^{K+\frac{i-2}{N}} = [\ -\mathbf{M}_F + (1-\gamma)\,\Delta t_f\,\mathbf{C}_F]\mathbf{u}^{K+\frac{i-2}{N}} + \left(-\beta + \gamma - \frac{1}{2}\right)\Delta t_f^2\,\mathbf{K}_F\{\mathbf{RS}\}^{K+\frac{i-2}{N}} \quad (14)$$

in which the restoring forces of the FE-domain are calculated from elements as

$$\{\mathbf{RS}\}^{K+\frac{i-1}{N}} = \sum_{e=1}^{elements} \int_{v_e} [\mathbf{B}_e]^T \{\sigma_e\}^{K+\frac{i-1}{N}}\, dv_e \quad (15)$$

$$\{\mathbf{RS}\}^{K+\frac{i-2}{N}} = \sum_{e=1}^{elements} \int_{v_e} [\mathbf{B}_e]^T \{\sigma_e\}^{K+\frac{i-2}{N}}\, dv_e \quad (16)$$

with the element stresses $\{\sigma_e\}^{K+\frac{i-1}{N}}$ and $\{\sigma_e\}^{K+\frac{i-2}{N}}$ being the converged ones at the time specified by the superscripts (Appendix). The interface nodal forces $\{\mathbf{RB1}\}^{K+\frac{i}{N}}$ are defined in Eq.(5) but $\{\mathbf{RB1}\}^{K+\frac{i-1}{N}}$ should be replaced by

$$\{\mathbf{RB1}\}^{K+\frac{i-1}{N}} = -\,K_{BB}\begin{Bmatrix} 0 \\ \mathbf{u}_I \end{Bmatrix}^{K+\frac{i-1}{N}} \quad (17)$$

The convergence criterion used here is

$$\frac{\left|\Delta \mathbf{u}_{(j)}^{K+\frac{i}{N}} - \Delta \mathbf{u}_{(j-1)}^{K+\frac{i}{N}}\right|}{\mathbf{u}^{K+\frac{i}{N}}} \le \varepsilon \quad (18)$$

Besides the hysteric damping a small amount of viscous damping is additionally included. In this study, the element-wise viscous damping matrix **c** is defined as proportional to the element stiffness matrix **k** and the mass matrix **m**, which leads the Rayleigh damping of

$$\mathbf{c} = a\mathbf{m} + b\mathbf{k} \quad (19)$$

where a and b are constants. It is assumed that since the kinematic energy is dominantly contained in the lowest vibration mode, the average damping ratio ζ within elements is given by the constants

$$a = \zeta\omega_1,\ b = \zeta/\omega_1 \quad (20)$$

where ω_1 is the first natural frequency to be determined from the solution of eigenmodes decomposition of the FEM soil domain under the fixed condition along the interface with the far field.

Along with the nonlinear analysis, a corresponding linear analysis is also conducted in which an equivalent viscous damping is introduced to account for the hysteric energy dissipation. The nonlinear computations are therefore preceded to determine the average strain level produced throughout the FEM meshes over the duration time. Then the areas of resulting stress-strain hysteresis are traced to obtain the equivalent damping ratios for the linear analysis. This procedure was proposed by Marsh *et al.*[13] and referred to as a scaled damping. Thus determined damping matrices for each element are assembled into the global matrix by the standard finite element formulation.

4. RESULTS AND DISCUSSION

The BEM-FEM model is shown in **Fig.4** along with the soil material numbers for different portions of the model. The meshing is carried out for the elements size to be smaller than one-fifth of the smallest wave length concerned by assuming the maximum frequency is around 10 Hz. The location of P_1 roughly corresponds to the coast, P_2 being taken as the origin in the x-direction in the succeeding analysis, to the fall down site of the Fukae section of the Hanshin Expressway viaduct and P_5 to the KBU. The sever nonlinearity is expected for the soft soil around the coastal area, and gradually decreased toward the foot of the Rokko mountains.

Table 1 Soil parameters used for nonlinear analysis

Material No.	Density (t/m^3)	Shear wave velocity (m/s)	Refrence strain γ_r
1	1.7	120	0.00060
2	1.7	140	0.00080
3	1.8	160	0.00080
4	1.8	180	0.00150
5	1.8	200	0.00200
6	1.8	220	0.00250

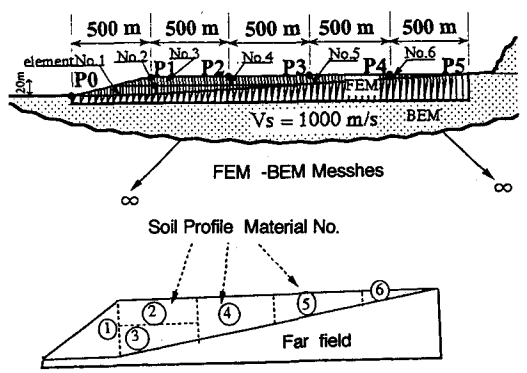

Fig.4 FEM-BEM descretization for numerical analysis

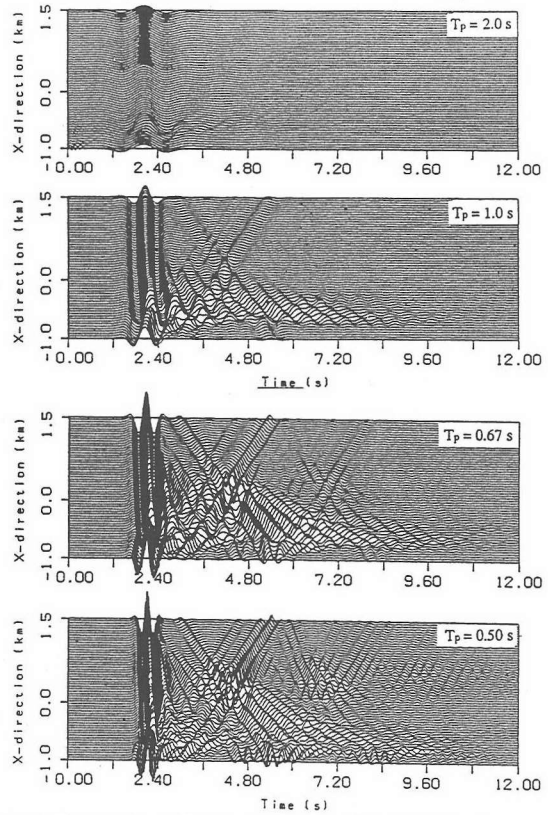

Fig.5 Horizontal nonlinear acceleration time histories due to incident Ricker wavees of different periods.

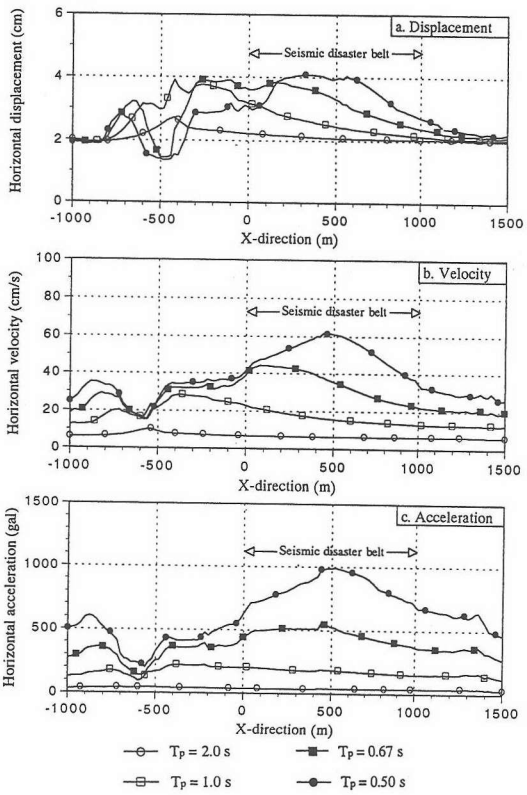

Fig.6 Maximum horizontal nonlinear responses due to incident Ricker waves of different periods.

The soil properties for the site analysis is referred to the bore hole test data. The shear velocity is estimated from the N-value by the formula[14)]

$$V_S = 68.79\, N^{0.171} \times H^{0.199} \times E \times F \qquad (22)$$

where H is depth, E=1.0 for alluvium 1.303 for diluvium F=1.0, 1.056, 1.066, 1.135, 1.448 for clay, fine sand, medium sand, coarse sand, and gravel, respectively. The resulting values are listed in **Table 1**.

The Hyogo-ken Nanbu Earthquake acceleration records showed different periodic contents at different sites. The Kobe University (KBU) records which is located on a firm soil, showed a predominant period longer than 1.0 s reflecting the close-by fault rapture. The Japan Meteorological Agency (JMA) records, which are considered to be affected by the local shallow alluvium site condition had a predominant period shorter than 1.0 s. Therefore, in order to grasp the global response characteristics of the soil deposits, first Ricker waves of different characteristic periods T_p are assumed for the input motions at the far field. Note that the Ricker waves have specific period contents that distribute densely around the period T_p ; namely, in the range $0.3<T/T_p<5$ (in frequency $0.2<f/f_p<3$Hz). The incident wave for the analysis is prescribed by the displacement.

Fig.5 shows the resulting response time histories for horizontal acceleration along the soil surface. We note the horizontally traveling waves generated by the edge as observed in the linear analysis,[3),4)] especially for short period motions. The difference arises in the amplification at the coastal area in the present analysis in such a way that the nonlinear behavior subdues the response. More specifically, the soil nonlinearity reduces the vertically propagating waves and the resonance of the surface soil deposits. The surface waves, although it exists substantially near the surface, get only a slight effect by the soil nonlinearity.

Fig.6 gives the maximum horizontal response profile for the cases in **Fig.5**. Except that the maximum responses have significant reduction in the coastal area, the similar response trend is obtained to those from the linear analysis,[3),4)] namely, the short period motions are more amplified than the long period motions. The

maximum amplification is centered to the heavily damaged area from zero to several hundreds meter in x-direction as indicated in **Fig.6**. Therefore, we may state that this response trend is due to the site characteristic and is less affected by the nonlinear soil behavior.

Next, for earthquake response simulations, the following different incident seismic motions are considered:

(1) Based on the outcropping condition, one half of the KBU records to represent the long period motions.

(2) Deconvoluted motions of the JMA records, to represent the short period motions. For this information, see the authors' previous paper. [4)]

(3) A set of Ricker waves which indicate the long period motions to simulate the major components of KBU records.

(4) A set of Ricker waves of short period motions to simulate the major components of JMA records.

Fig. 7 depicts the response time histories for the decomvoluted JMA motions. Since the displacement component is primarily governed by the long period motions, the short period motions are not so clear being embedded in these long period motions. However, in the velocity and acceleration components the short period vertically propagating motions become appreciable in this order. The motions at the coast are forced to be longer in period and reduced in amplitude, when compared to the linear results[3),4)], due to the nonlinear behavior. The horizontally traveling waves from the Rokko mountains toward the coast can also be observed as in the previous linear response analysis. Although the time histories for other input motions are omitted, these response trends are almost the same with those in the linear case.

Fig. 8 gives the computed maximum responses profile. The case for the deconvoluted JMA records results in the higher responses than other cases and the amplification is centered to the observed disaster belt zone with the maximum value more than 1,000 gals in acceleration and around 100 kines in velocity. These response values agree well with the estimation from other investigators,[15),16)] as marked in the same figure by symbols although the soil models for analysis differ from the present model. The observed data at Fukiai Osaka Gas station are also included in **Fig.8** at a possible location, and the JMA data (820 gals and 90 kines) are supposed to be located at x=1,000m in the same figure. Those comparable values substantiates the present simulation. The KBU data are referred to later. The short period motions gives the same acceleration

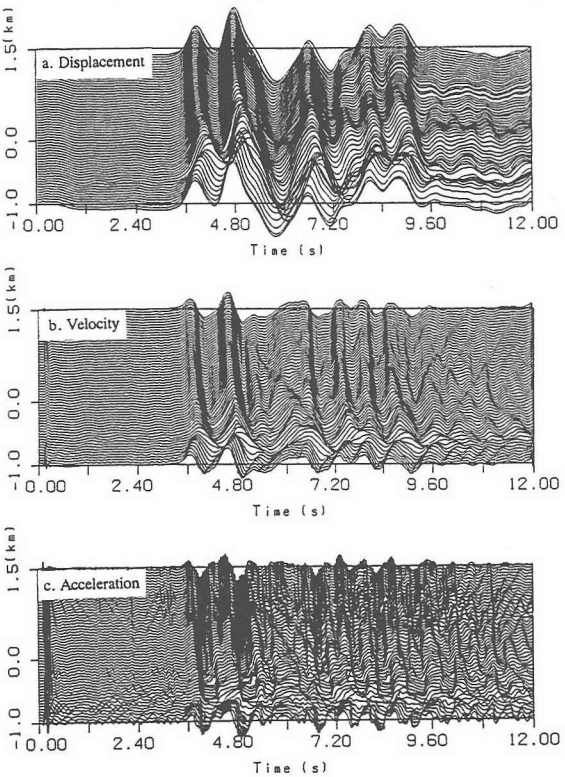

Fig.7 Alluvium surface response time histories due to the decomposed JMA input motions.

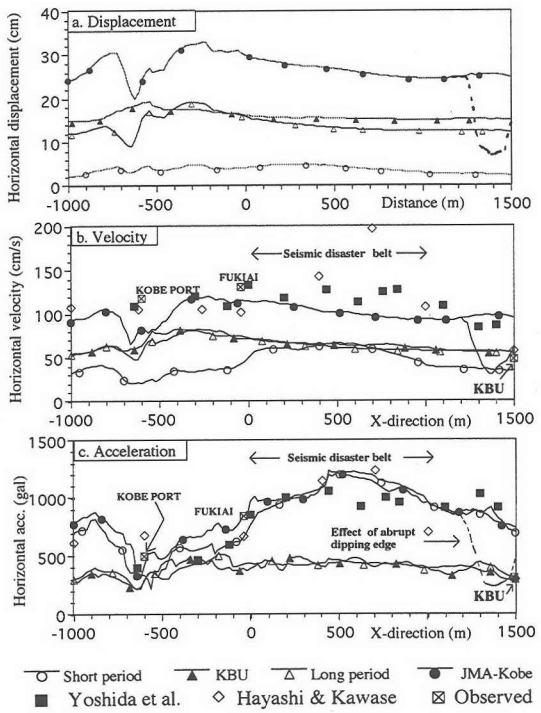

Fig.8 Maximum horizontal nonlinear responses due to different input earthquake motions.

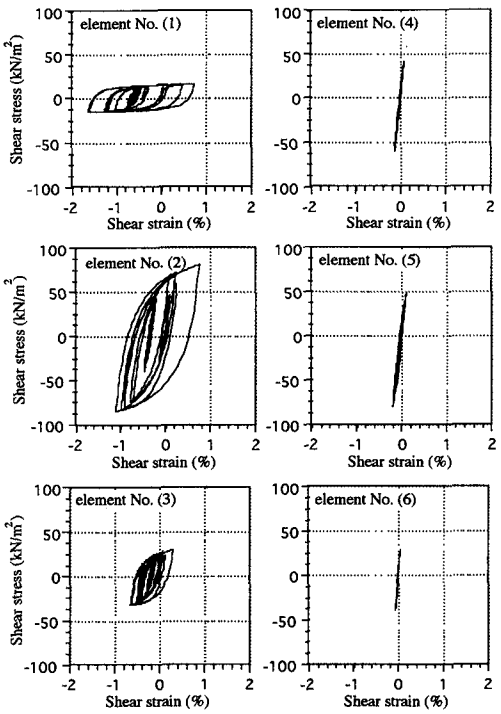

Fig.9 Stress-strain hysterisis curves at representative nodes

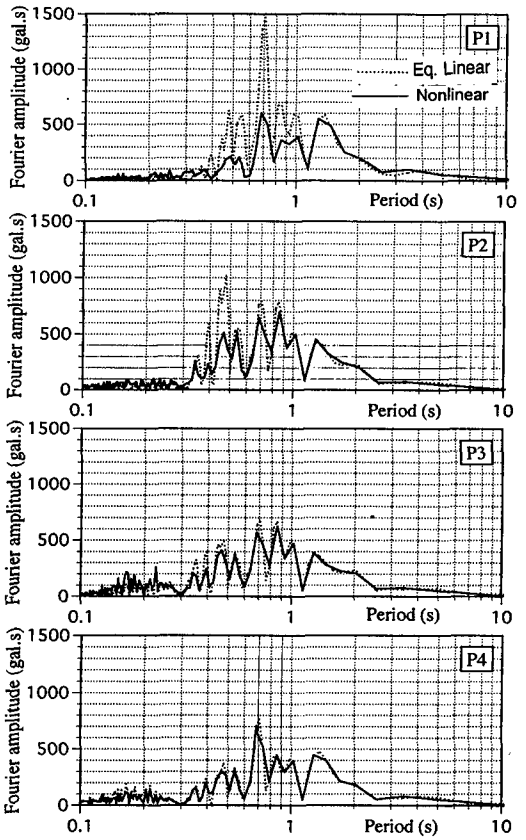

Fig.10 Fourier transforms of linear and nonlinear responses at different locations due to the JMA input motions.

profile with the decomvoluted JMA-Kobe but the lower velocity and smaller displacement response than it. This difference is attributed to the fact that we use the same input acceleration amplitude for the short period motions with the deconvoluted JMA record but with the respective integrated velocity and displacement. The KBU record and the long period motions results in much lower values than other input motions with almost the same response value all along the soil surface. This trend was noted in the linear analysis.[3),4)]

In **Fig.8** the acceleration at P_5 supposed to be the foot of the Rokko mountains are larger than the actually observed value 430 gal at the KBU record. This can be modified as in what follows by considering additionally the deep stiff Osaka Group layers. Concerning the abrupt dipping of the underlain base rock at the foot of Rokko mountains, we have found in the pervious work[3),4)] that the deamplification occurs in horizontal component in the range around 300 m from the edge while the amplification in the vertical component. Since the soil behavior at this area remains almost linear, we may include such effect by calibrating the current response accordingly. Then, the modified responses turns out compatible with the observation at the KBU as indicated by the dashed lines.

Fig.9 depicts the stress-strain hysterisis of the selected elements at representative locations indicated in **Fig.4**. We observe a severely nonlinear behavior of the strain level reaching 10^{-2} at the coastal area (around the location P_1) outside the disaster belt zone whereas at other area including the disaster belt zone the less nonlinear behavior of the strain 10^{-3} or less. Judging from these results we may state that the sever nonlinearity has occurred and therefore the high hysteric damping have been associated with at the coastal area. This area in fact suffered sever liquefaction during the earthquake and its response may better be explained by the effective stress analysis with the change of pore water pressure.

As mentioned in the **Section 3**, we approximated the hysteric damping by an equivalent viscous damping ratio for the purpose of the linearization. The calculated damping ratio varies from 5% at low strain level of 10^{-4} up to 25% at high strain level of 10^{-2} for the coastal area. For other areas, the ratio is between 3% at low strain and 10% at high strain level, depending on the locations addressed.

The frequency contents of the surface motions are investigated. **Fig.10** shows the frequency contents of acceleration response at representative locations shown in **Fig.4** for both the nonlinear and the equivalent linear responses with scaled damping due to the JMA input motions. At the coastal area, the Fourier amplitude in the short period range (less than 1. s) is highly reduced by the nonlinear behavior while for the long period range it has a very slight effect. At other locations, the amplitudes and the predominant periods have small difference between the equivalent linear and the nonlinear behaviors.

5. CONCLUSION

As a succeeding work to the previous FEM-BEM linear analysis, the authors developed a computer program that can simulate the 2-dimensional nonlinear soil response for an incidence of earthquake motions.

As an application of the system, in this paper the authors focused the nonlinear behavior of Kobe's alluvium soils to interpret the disaster belt of JMA intensity, from which the following conclusions may be stated:

(1) During the Hyogo-ken Nanbu Earthquake, the sever nonlinear response seems to have occurred at the coastal area, reducing the unrealistic high acceleration at the coastal area in linear analysis whereas less degrees of nonlinear response in other area including the disaster belt zone. The obtained response for the deconvoluted JMA record leads an expected acceleration profile compatible with the actual seismic damage degrees in Kobe.

(2) The high acceleration was still attained at the severely damaged belt zone in use of the decomvoluted JMA records while almost no amplification for the alluvium in use of the KBU records whose period contents mainly longer than 1 s. Such long input motions may not be concerned with the present alluvium amplification which means with the strain generation inside it.

(3) The Fourier spectra of the nonlinear ground surface acceleration suggests that the short period motions less than 1 s might be affected by the nonlinear soil behavior significantly whereas the longer motions than this might be almost not.

(4) The linear response analysis in terms of a scaled damping for appropriately chosen soil properties resulted in the response features similar with those from the previous linear analysis but with less amplified response values at the coastal area. It also gave an adequate explanation of the site response.

Appndix: Iterative solution for nonlinear response

Takemiya and Ishiyama[10] showed a procedure to obtain the out-of-balance stress vector in the two-dimensional nonlinear soil dynamic analysis. They assumed that the mean stress σ_m and the diretion angle Ψ of the principal stresses remain unaltered during the nonliner stress adjustment. See Fig.A.1.a. The resulting Mohr's circle of the nonlinear shear tress is then represented by the circle B in the figure aftrer iteration.

Here, we assume that the normal stresses are kept linear in variation while the shear stress τ_{xz} varies nonlinear according to thre strain level γ_{xz}. The out-of-balance is therefore described by

$$\Delta\sigma_{e,u}=\begin{Bmatrix}\Delta\sigma_{xe,u}\\ \Delta\sigma_{ze,u}\\ \Delta\tau_{xze,u}\end{Bmatrix}=\begin{Bmatrix}0\\ 0\\ \tau_{xze,n}-\tau_{xze,l}\end{Bmatrix}$$

The normal stresses follow the variation of the shear stress to satisfy the equilibrium during the iteration. Therefore, the nonlinear effect is to be taken into account implicitly. The preseent sheme is simpler than the previous one, althogh both of which converge to the same value within a specified accuracy. The iteration process for evalutating the nonlinear shear stress for individul elements is self evident in the illustration in Fig.A.2 The quasi-external forces are equivalent to the out-of-balance stresses of the whole system at the current iteration.

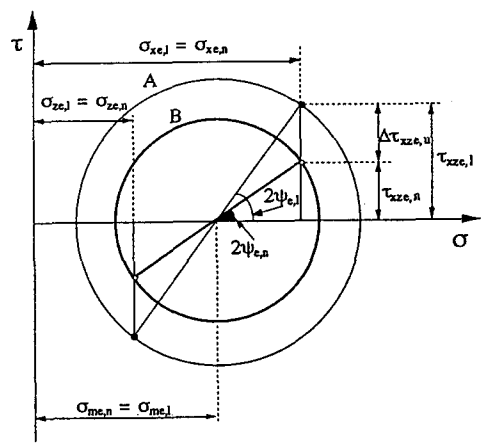

Fig. A.1 Modified Mohr's circle for nonlinear shear stress

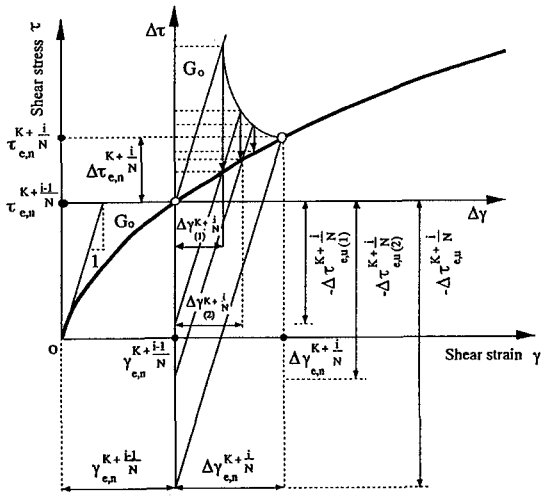

Fig. A.2 Iterative evaluation of nonlinear shear stress

REFERENCES

1) Ishikawa, K., Mizoguchi, S. and Ooshika, A., Geology in Kobe area and investigation of the disaster on the 1995 south Hyogo Great Earthquake, *J. Japan Society of Engineering Geology*, 36-1, 62-80, 1995.7.
2) Takemiya, H.: Effect of irregular soil profile on strong ground motions, pp.15-25, *The 1995 Hyogoken-Nanbu Earthquake, -Investigation into Damage to Civil Engineering Structures-, Committee of Earthquake Engineering*, Japan Society of Civil Engineers, June 1996.
3) Takemiya, H. and Adam, M.: Why the heaviest damages occurred in Kobe during the Hyogo-ken Nanbu Earthquake, Japan 1995, *The Kobe Earthquake: Geodynamical aspect,* edited by Brebbia, C.A., Computational Mechanics Publication, Southampton, UK, pp.39-58, 1995.
4) Takemiya, H. and Adam, M.: Seismic wave amplification due to topography and geology in Kobe during Hyogo-ken Nanbu Earthquake, *Structural Eng./Earthquake Eng.*, JSCE, Vol.14, No.2, 129s-138s, 1997 July.
5) Kobe City Office: Ground of Kobe (*Kobe no Jipan*), 1982. (in Japanese)
6) Takemiya, H., Adam, M. and Yasui, Y.: Transient seismic response of irregular sites, Proc. of 3rd Int. Conf. on Recent Advances in Geotech. Earthqu. Eng. and Soil Dynamics, St. Louis, MO, USA, 1995.4.
7) Bathe, K.: Finite Element Procedures in Engineering Analysis, Printice-Hall, Englewood Cliffs, NewJersy, 1982
8) Masing, G.: Eigenspannungen und Verfestigung beim Messing, Proceedings, Second International Congress of Applied Mechanics, pp. 332-335, 1926.
9) Hardin, B. O. and Drnevich, V. P.: Shear Modulus and Damping in Soils: Design Equations and Curves, J. *Soil Mech. and Foundation Division*, ASCE, Vol. 98 No. SM7, pp. 667-692, 1972.
10) Takemiya,H. and Ishiyama, M., Nonlinear seismic response of an alluvium of non-flat base, Proc. Japan Society of Civil Engineers, No.477/I-25, 73-81, 1993.10.
11) Touhei, T. and Yoshida, N.: Dynamic response analysis of ground using a coupled finite element and boundary element method in time domain, *Proc. JSCE,* No.410/I-12, pp.395-404, 1989.10
12) Abe,K. and Yoshida, Y.: Application of time domain boundary finite element hybrid method to dynamic analysis of sediment filled valleys, *Proc. JSCE,* No.428/I-15, pp.107-116, 1994.4.
13) Marsh, J., Larkin, T., Haines, A. and Benites R.: Comparison of linear and nonlinear responses of two-dimensional alluvial basins, Bulletin of Seis. Soci. of America, Vol. 85, No. 3, pp 874-889, 1995
14) Ohta, Y. and Goto,N: Estimation of S-wave velocity in terms of characteristic indices of soil, *Butsuri-Tanko* 29, No.4, pp.34-41.
15) Yoshida, N. *et al.*: Nonlinear behavior of ground during the 1995 Hyogo-ken Nanbu Earthquake, *Proceedings of the International Workshop on Site Response subjected to Strong Earthquake Motions, Yokosuka, Japan, pp. 374-389,* 1996.
16) Hayashi, Y. and Kawase, H. Strong motion evaluation in Chuo Ward, Kobe, during the Hyogo-ken Nanbu Earthquake, J. Struct. Constr. Eng. AIJ, No.481, pp37-46. March., 1996.

(Received September 10, 1996)

FEM-BEMによる2次元非線形地盤解析：兵庫県南部地震における神戸のケース

竹宮宏和 ・アダム マヘール

兵庫県南部地震(1995.1.17)により神戸を中心に震度7の震災帯が形成された.その原因究明のため,著者らは表層地盤の不整形性に注目して2次元非線形FEM-BEMによるコンピュータ・シミュレーション法を開発した.そして神戸の地盤物性の不規則分布,強震時の地盤の非線形性を考慮した解析を実施した.その結果,海岸寄りは強い非線形応答により加速度は低減し,震度7の震災帯では弱い非線形性により加速度は大きく地震時の様相と思われる最大値分布となった.これに関係した卓越波は周期が1秒以下である.シミュレーション結果と観測値の対応はよい.速度応答においても同様である.併せて等価線形解析の応答値も示した.震度7の震災帯の出現には上述の地盤増幅効果が原因したと思われる.